Characterization of Moisture Transport and Its Effect on Deformations in Jointed Plain Concrete Pavement

Ya Wei and Will Hansen

Many aspects of concrete durability and performance are influenced by moisture conditions in concrete. Although the importance of moisture effect on concrete pavement has been widely recognized, moisture deformations and stresses were usually ignored in pavement analysis because of a lack of comprehensive understanding of moisture transport properties and difficulties in characterizing their magnitudes. Three moisture transport processes and their effects on internal relative humidity distributions along slab depth, thought to be the major factors affecting concrete pavement deformations and stresses, are discussed. The processes are drying shrinkage and associated nonuniform humidity distribution within the top few inches of a slab, self-desiccation caused by hydration and associated uniform humidity distribution within the entire slab cross section, and water absorption caused by capillary suction and associated nonuniform humidity distribution within the bottom portion of the slab. Experiments and simulations showed that the total humidity loss was a result of self-desiccation and external drying; excessive warping in jointed concrete pavement was caused by simultaneous top surface drying and bottom surface water absorption. Pore discontinuity caused capillary suction at the bottom surface to produce a steep moisture gradient and associated moisture warping. A new methodology was proposed for characterizing moisture-related deformations in slab on ground on the basis of a relationship of shrinkage versus relative pore humidity for concrete. This relationship was obtained from autogenous shrinkage results, which related free shrinkage deformations of a concrete to its internal humidity volumetric aggregate concentration. The proposed methodology provides for a simple postprocessing of moisture-related deformations in slabs on grade.

It is generally recognized that curling (i.e., temperature gradient effect) and warping (i.e., moisture gradient effect) properties of slabs on grade combined can have a detrimental effect on pavement performance (*1*, *2*). Whereas curling effects are fairly well understood, a fundamental understanding of moisture warping in the context of wetting at the bottom surface of a slab is lacking. The cause of moisture warping is traditionally attributed to differential drying when slab top surface is exposed to external drying. However, practical experience clearly demonstrates that excessive moisture warping uplift develops in slabs on grade if conditions of poor drainage and saturated soils are prevalent (*3*, *4*).

Therefore, besides differential drying from slab top surface, two other moisture transport processes may be involved in creating a large moisture gradient along slab depth and cause additional slab warping. One is self-desiccation associated with cement hydration, and the other is water absorption at the slab bottom. During cement hydration, capillary pore water is consumed for chemical reactions to proceed; this results in a reduction in capillary pore humidity, known as self-desiccation (*5*). Self-desiccation activates internal pore stresses and associated autogenous deformation characterized by a uniform reduction in bulk volume of concrete. As long as the concrete surfaces are sealed during hydration, autogenous shrinkage is uniform, and thus no warping develops. Disconnection of the capillary pore network is another fundamental factor associated with cement hydration (*6*). For a slab resting on a saturated base due to ineffective drainage, water is therefore detained at the slab bottom. Thus, water absorption occurs and causes a steep moisture gradient in the lower region of a slab as a result of discontinuity in the pore network. Water absorption is a process of water front that moves through the concrete from capillary suction pressure within pore spaces of the concrete (*7*). It was found that capillary absorption decelerates as cement hydration increases (*8*).

The aim of this paper is to investigate the role of moisture transport properties on slab uplift, traditionally related to temperature effects (built-in curl and daily curl) and to provide a methodology for quantifying the effects of moisture warping. Findings from this work can significantly improve design methods for slabs on grade and construction procedures.

MOISTURE TRANSPORT IN SLABS ON GROUND

Self-Desiccation

Self-desiccation exists in cementitious materials as long as cement hydration proceeds. Self-desiccation causes uniform reduction of internal relative humidity (RH), and the extent depends on the initial water–cement (w/c) ratio and degree of hydration of the cementitious materials. In this study, the internal RH developments of cement pastes with Blaine fineness of 4,290 cm^2/g and w/c ratios of 0.35, 0.4, and 0.45 were simulated using Hymostruc for sealed-curing conditions. Hymostruc is a microstructural-based model that can predict internal humidity reduction for different cement compositions and has been proved as a reliable predictor for internal pore humidity of cementitious materials (*9*).

Y. Wei, Department of Civil Engineering, Tsinghua University, Qinghua Yuan Street, Beijing 100084, China. W. Hansen, Department of Civil and Environmental Engineering, University of Michigan, 2350 Hayward Street, 2340 G. G. Brown Building, Ann Arbor, MI 48109. Corresponding author: Y. Wei, yawei@tsinghua.edu.cn.

Transportation Research Record: Journal of the Transportation Research Board, No. 2240, Transportation Research Board of the National Academies, Washington, D.C., 2011, pp. 9–15.
DOI: 10.3141/2240-02

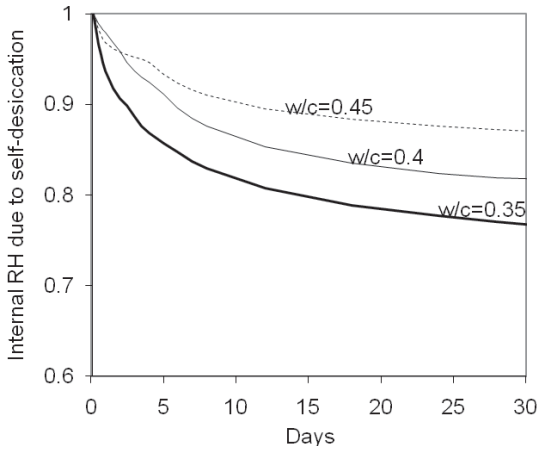

FIGURE 1 Development of internal RH of ordinary Portland cement paste resulting from self-desiccation at w/c ratios of 0.35, 0.4, and 0.45.

Self-desiccation proceeds with increasing degree of cement hydration. As shown in Figure 1, internal humidity drops rapidly within the first few days, with the greatest reduction in lower w/c ratio = 0.35 cement paste. The lower the internal humidity, the less will be the free capillary water held in hydrating cement paste. Thus, at low internal humidity, the amount of anhydrous cement particles that are exposed to water and space available for hydration products are significantly reduced. This will limit further cement hydration and thus further reduce internal humidity. It is well established that self-desiccation ceases when internal humidity is reduced to a range of 70% to 75% (*5, 10, 11*).

In concrete pavement, self-desiccation results in a uniformly distributed humidity profile along pavement depth, as illustrated in Figure 2 for a 254-mm (10-in.) -thick slab. As self-desiccation proceeds with increasing degree of hydration, humidity profiles push to lower values over time. This will macroscopically result in joint contraction, which if restrained causes tensile stress. Figures 1 and 2 suggest that joint contraction movement is pronounced during early ages as internal RH drops rapidly during this time period, and the lower the w/c ratios, the greater joint movement would be.

External Drying

External drying occurs when moisture is lost from the concrete surface to the environment. This type of drying is a diffusion-controlled process in which moisture moves from regions where it is plentiful to regions where it is scarce, governed by nonlinear diffusion equation where moisture flux is proportional to moisture gradient. In mass concrete, external drying is an extremely slow process. It will take approximately 1 year for the outer 225-mm (9-in.) concrete to reach moisture equilibrium (*12*). Therefore, external drying affects only a shallow portion of the pavement depth. Figure 3 shows the simulated humidity profiles along a 254-mm (10-in.) -thick slab with the top surface exposed to a 50% RH environment for 28 days after sealed curing for 28 days. No moisture exchange through the slab bottom was assumed in modeling. As illustrated in Figure 3, during the sealed curing period (first 28 days), the RH profiles were uniformly distributed along slab depth, and no moisture gradients were observed. The uniformly distributed RH profiles pushed to the lower values and reached 87% at the end of sealed curing period. However, with exposure of the top surface to the environment, external drying occurs as a result of the lower RH of environment than in the concrete interior. This results in a RH reduction within the top portion of slab thickness. After 28 days of exposure to drying, only 5 to 10 cm (2 to 4 in.) in depth from the top was affected, which agrees with the findings by Janssen for the case of a long drying time period (*13*). No matter if there is external drying or not, a uniform RH reduction always exists as long as cement hydrates. Thus, the total moisture loss is a result of both self-desiccation and external drying. As seen in Figure 3, there is a uniform RH reduction from self-desiccation during the external drying period from the 28th to 56th day.

Water Absorption

In addition to moisture loss from self-desiccation and external drying, water ingress into the concrete through absorption is also more

FIGURE 2 Humidity profiles along slab depth in concrete pavement with w/c of 0.45 under sealed curing conditions.

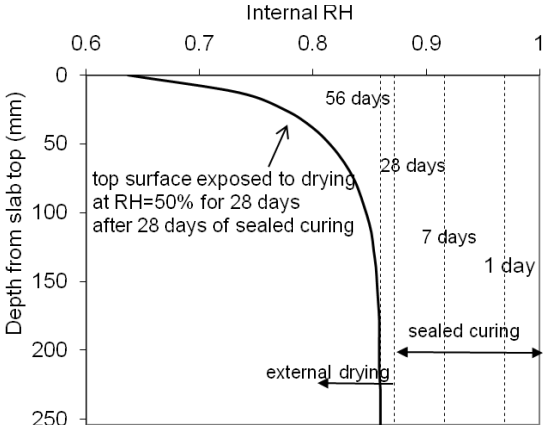

FIGURE 3 Humidity profiles along slab depth in concrete pavement with w/c of 0.45 and top surface exposed to drying after 28 days of sealed curing.

representative of conditions encountered in the field. Capillary suction within the pore space of the concrete is the major driving force for water absorption. If one considers a concrete initially unsaturated, once it is in contact with liquid water, water absorption is accomplished by an initial instantaneous surface suction, a subsequent capillary suction, and a later water diffusion at smaller (gel) pore level. Neithalath's study indicates that approximately 70% of the overall water absorption results from suction, and approximately 30% is attributed to diffusion (*14*).

Modeling of capillary suction in unsaturated concrete is rather complex, for the relevant transport properties vary and depend on many factors. In this study, the effect of capillary suction on RH development was modeled by using a surface factor that characterizes the moisture flux through the wetting boundary and moisture transport into the concrete. The surface factor selected in modeling was calibrated by matching the predicted warping deformations to the measured values of concrete beams tested, using a new experimental program adopted in this study.

Figure 4 shows the simulated RH profiles along the depth of a 254-mm (10-in.) -thick slab. The slab was first sealed cured for 28 days, and then the top surface was exposed to drying at RH of 50%; the bottom surface was in contact with moisture (assuming RH of 100% in modeling). It can be seen that the combined effect of both drying at the top surface and wetting at the bottom surface results in a greater differential RH gradient compared with the case of drying at the top surface alone (see Figure 3). It was anticipated that such a moisture gradient would cause significant warping in concrete pavement. This agrees with observations and experiences that when a floor slab or highway pavement is exposed to water at the bottom surface while the top surface dries and shrinks, excessive warping deformation (5 ~ 6.4 mm) can develop within months after construction (*15*).

According to Figure 4, both bottom surface wetting and top surface drying affect an area approximately 10 cm (4 in.) in depth from surfaces, consistent with Beddoe and Springenschmid's findings that the majority of moisture transport is limited to a surface region of less than about 8 cm (3.1 in.) (*16*). For the case of slab bottom absorption, it is suspected in this study that water absorption through capillary pores is hindered because of the disconnection of the capillary pore network from cement hydration. Moisture is therefore detained in the lower region of the slab subject to bottom wetting. Once capillary discontinuity has developed, any slab thicker than about 8 to 10 cm is subject to a nonlinear moisture gradient if one of the free surfaces is exposed to moisture.

FROM INTERNAL RELATIVE HUMIDITY TO SHRINKAGE DEFORMATIONS

The variation of internal humidity promotes joint movement and warping deformations in slabs on the ground. To improve the design of concrete slabs, the material behavior under moisture-related conditions has to be characterized more precisely. Equations have been established to characterize the relationship between internal humidity and shrinkage deformation (*17*, *18*). However, most of these relationships were based on drying shrinkage results of concrete samples. It is well known that drying shrinkage is hindered by not only external but also internal restraints. Ideally, local shrinkage is directly related to its local pore humidity (*19*). Owing to the restraints, however, this is not the case when concrete is subject to external drying. Thus, difficulties exist in relating the shrinkage value of bulk drying (macroscopically measured) of a concrete to its internal humidity that varies everywhere. In this study, a new method is presented for characterizing shrinkage deformation as a function of pore humidity of concrete from autogenous shrinkage results. Autogenous shrinkage is a material-level deformation, and thus no size effect is involved owing to its uniform properties of RH distribution.

One-dimensional autogenous shrinkage was first measured on sealed paste samples, with a double-walled, water-cooled, stainless steel apparatus. The detailed test procedure can be found in Wei et al. (*20*). The same materials as the one for RH prediction were used (Figure 1). Then, the measured autogenous shrinkage results were plotted versus simulated RH for each paste mix. A unique correlation between paste autogenous shrinkage development and pore humidity reduction was observed, which is approximately independent of the w/c ratio (0.35, 0.4, and 0.45), as illustrated in Figure 5. A

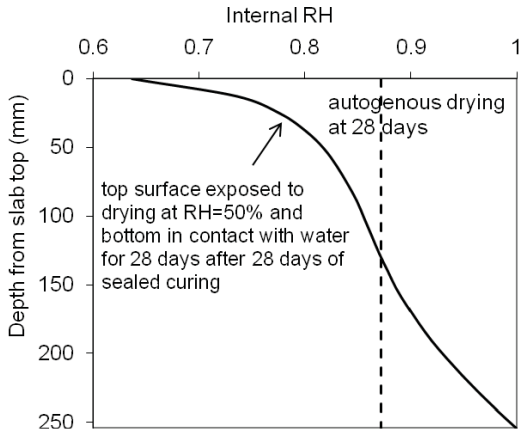

FIGURE 4 Humidity profiles along slab depth in concrete pavement with top surface exposed to drying and bottom surface in contact with moisture after 28 days of sealed curing.

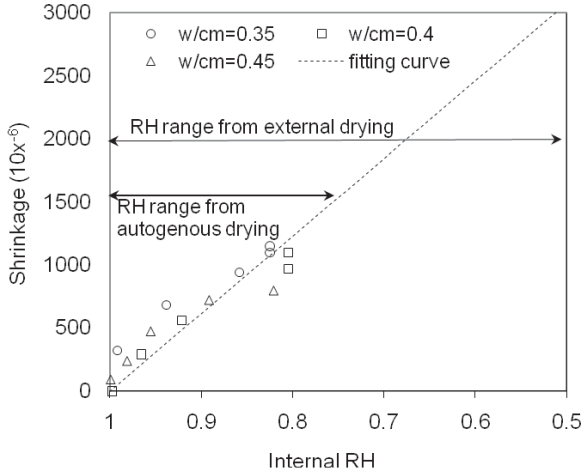

FIGURE 5 Relationship between paste shrinkage deformation and internal RH based on autogenous shrinkage results.

linear regression equation (Equation 1) with R^2 value of .89 was obtained for quantifying autogenous shrinkage of a portland cement paste ϵ_P within the pore humidity range of 100% to 80%:

$$\epsilon_P = 6150(1 - \mathrm{RH}) \times 10^{-6} \quad (1)$$

This agrees with Jonasson et al. that a linear relation between autogenous shrinkage and pore humidity exists (*19*).

It has been suggested that autogenous shrinkage is a special class of drying shrinkage (*12*). Drying shrinkage spans a wider RH range and is typically measured at 50% RH, while on the contrary autogenous shrinkage is limited to a more narrow RH range (not less than 70%). It is generally thought that drying shrinkage is most likely related to changes in surface tension of the solid gel particles resulting from absorption and desorption of water layers, and autogenous shrinkage is primarily controlled by capillary tension in pore fluid. In spite of the difference in driving forces, drying shrinkage and autogenous shrinkage are both responses to pore RH changes. Therefore, it is acceptable to extend the linear curve of shrinkage versus pore RH obtained from the autogenous shrinkage result to the lower RH range to account for the drying shrinkage effect as shown in Figure 5. From Equation 1, it is calculated that shrinkage at 75% RH is 0.54 of the shrinkage at 50% RH. This is consistent with shrinkage results of a 0.30 w/c concrete in which the autogenous to drying shrinkage ratio of 0.5 has been reported (*21*).

The present findings suggest that an expression such as presented in Equation 1 can be a unified model for shrinkage prediction in general. Because both autogenous and drying shrinkage are paste properties, the practicability of Equation 1 can be enhanced if it can be applied to predict concrete shrinkage. This is done by incorporating the Pickett model, which was originally developed for prediction of drying shrinkage (*22*):

$$\epsilon_C = \epsilon_P (1 - V_A)^n \quad (2)$$

where

ϵ_C = shrinkage of concrete,
ϵ_P = shrinkage of paste,
V_A = volume fraction of aggregates, and
n = correlation parameter controlled by aggregate restraining effects.

Equation 2 indicates that in concrete, the response of the paste to moisture loss is modified by the presence of aggregate (*12*). The shrinkage restraint factor n was found to be 1.68 based on autogenous shrinkage results of concrete and paste with w/c ratios of 0.35, 0.4, and 0.45, which is within the normal range of n values found for drying shrinkage typically varying from 1.2 to 1.9 (*22*, *23*).

In general, with Equations 1 and 2 combined, a concrete shrinkage equation looks like this:

$$\epsilon_C = [6150(1 - \mathrm{RH})](1 - V_A)^n \times 10^{-6} \quad (3)$$

From Equation 3, concrete shrinkage can be calculated if paste RH and aggregate content are known. Paste RH can be measured or predicted. Because Equation 3 was obtained from the case of uniform moisture gradient, and thus represents true materials-level shrinkage, it is suitable for quantifying moisture-related deformations in general as detailed in the next section for warping deformations in jointed plain concrete pavement (JPCP).

CHARACTERIZATION OF WARPING

Methodology of Warping Calculation

External drying and water absorption both can cause moisture and shrinkage gradients. The typical deformations under the two moisture conditions in a JPCP are illustrated in Figure 6. One case is drying at the top surface alone (Figure 6*a*), and the other case is simultaneous top surface drying and bottom surface wetting (Figure 6*b*) from detained water at slab bottom caused by ineffective drainage. Both cases cause a differential shrinkage gradient, with the top portion shrinking more than the bottom portion does. This consequently results in uplift of a slab corner and joint movement. However, the case of simultaneous top drying and bottom wetting causes much greater differential shrinkage gradient than the case of top surface drying alone, caused by the added effect from water absorption at the bottom surface.

Differential shrinkage will result in warping deformation in JPCP. The magnitude of warping can be quantified with an equivalent temperature gradient ΔT_e which causes the same magnitude of slab uplift as the moisture gradient does. This will allow using the finite element program for postprocessing of moisture-related deformations and stresses. In this study, ΔT_e was determined as follows. First, a slab with thickness of h is considered; the median plane lies in the xy plane, with z denoting the distance from this plane and z-axis pointing downward. Then, the strain moment is calculated based on the assumption of plane stress and those sections that are plane and perpendicular to the middle surface remain so after curling deformation. Assumed is that material properties (such as modulus) remain the same for both moisture deformation and thermal deformation. Thus, the moment caused by nonlinear RH (M_{RH}) gradient looks like this:

$$M_{\mathrm{RH}} = \frac{E}{1 - \nu} \int_{\frac{-h}{2}}^{\frac{h}{2}} \epsilon_C(z) z\,dz = \int_{\frac{-h}{2}}^{\frac{h}{2}} [6150(1 - \mathrm{RH}(z))](1 - V_A)^n \times 10^{-6} z\,dz \quad (4)$$

where

E = modulus of elasticity of concrete;
ν = Poisson's ratio of concrete;
$\epsilon_C(z)$ = local free shrinkage deformation of concrete at distance z from the median plane, which is a function of RH and volumetric aggregate concentration as expressed in Equation 3; and
RH(z) = local relative humidity at distance z from the median plane.

To obtain the equivalent temperature gradient ΔT_e, moment M_{RH} in Equation 4 is then assumed equal to moment M_T in Equation 5:

$$M_T = \frac{E \Delta T_e \alpha h^2}{12(1 - \nu)} \quad (5)$$

where α is the coefficient of thermal expansion of concrete. Thus, ΔT_e is found to be a function of internal RH, aggregate content, slab thickness, and coefficient of thermal expansion of concrete:

$$\Delta T_e = \frac{12}{\alpha h^2} \int_{\frac{-h}{2}}^{\frac{h}{2}} [6150(1 - \mathrm{RH}(z))](1 - V_A)^n \times 10^{-6} z\,dz \quad (6)$$

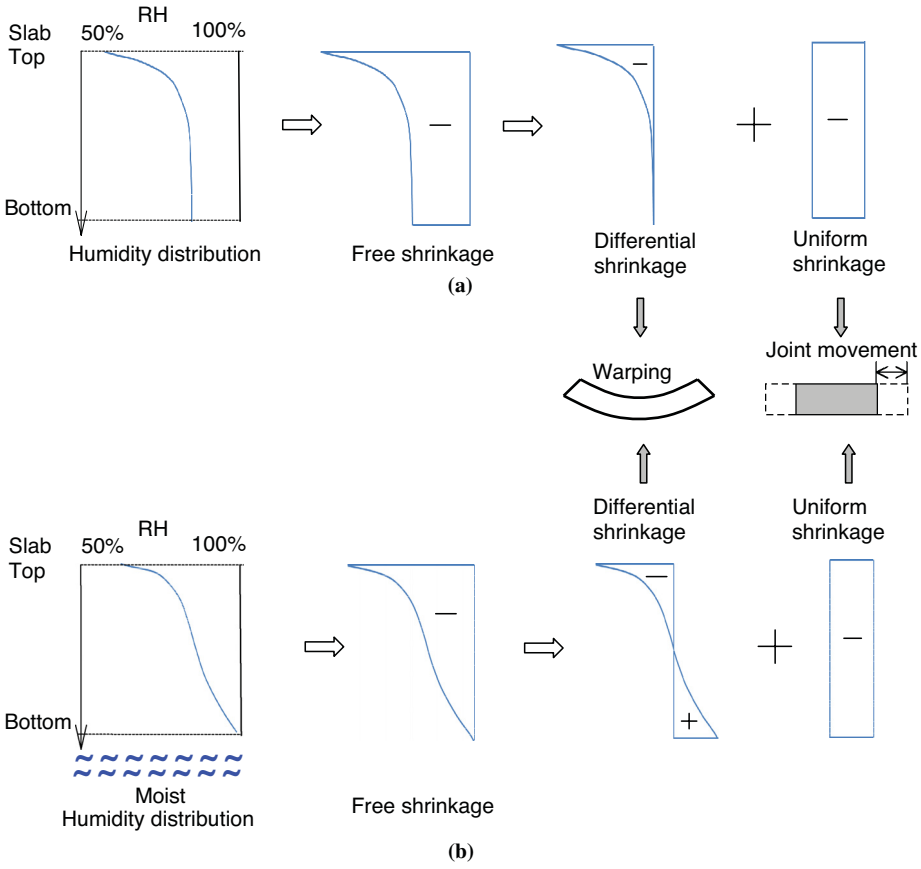

FIGURE 6 Typical moisture deformations in concrete pavement: (*a*) deformations when top surface is subject to drying and (*b*) deformations when top surface is subject to drying and bottom surface is subject to water absorption; shrinkage is negative and expansion is positive.

For moisture conditions shown in Figure 3 (external drying alone) and Figure 4 (combined drying and wetting), the calculated ΔT_e using Equation 6 are −7.2°C and −15.2°C, respectively, assuming $\alpha = 10 \times 10^{-6}$/°C and aggregate content by volume = 75%. It is seen that the added effect from bottom water absorption significantly increases the equivalent temperature gradient and consequently warping deformations.

Experimental Test

Beam warping tests were conducted to evaluate warping deformation under typical moisture conditions. This test setup was modified on the basis of work at Munich Technical University (*24*) which allows for exposing the beam to simultaneous drying from the top and water absorption at the bottom. As shown in Figure 7, beam length

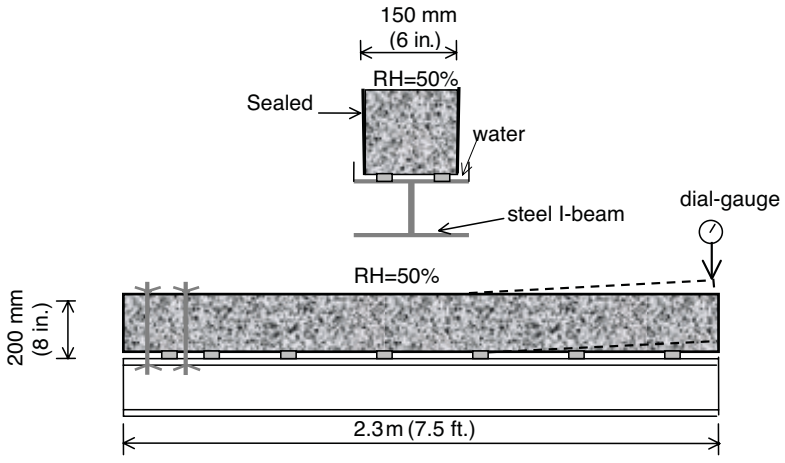

FIGURE 7 Uplift test of concrete beam under different drying conditions.

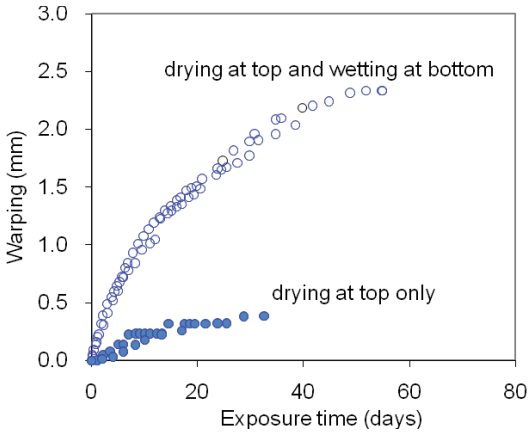

FIGURE 8 Measured beam warping under different moisture conditions.

was 2.3 m (7.5 ft), which is half of the JPCP slab length. The beam cross section is 200 mm (8 in.) high and 150 mm (6 in.) wide. One end of the beam is fixed, and the other end is free to lift up. A dial gauge was installed at the free end to record the magnitude of moisture warping over time. To facilitate a through-thickness moisture gradient, the other sides of beam were sealed using a waterproof paint. The entire setup was placed in an environmental chamber with RH of 50% and constant temperature at 23°C. Two beams were measured for each moisture condition. The test was initiated after 7 days of sealed curing.

Results of the beam warping test are shown in Figure 8. Beam uplift increases with exposure time. The uplift from combined external drying at the top surface and water absorption at the bottom surface far exceeds the uplift from external drying at the top surface alone. The experimental results suggest that water absorption at the bottom and capillary pore network disconnection might be the reasons for excessive warping found in JPCP. Water appearing at the bottom is probably a result of ineffective drainage.

Field Observations

A JPCP project constructed in 1996 is located on I-96, CS 47065, Livingston, Michigan. Each direction has three 3.66-m (12-ft) lanes with a 3-m (10-ft) portland cement concrete shoulder. Joint spacing is 4.6 m (15 ft). The slab thickness is 267 mm (10.5 in.). The concrete is a mix with blast-furnace slag coarse aggregate. The base is 10.2 cm (4 in.) in thickness and placed on a 7.6-cm (3-in.) -thick dense-graded aggregate separator course over a sand subbase. The subgrade soil consists of a well-mixed glacial till of sand to clay (*25*).

Surface elevation measurements along the outer edge lane marking of westbound lanes were taken on warm sunny days during June and July 2005. Slabs were found to be in a permanent upward concave condition for a series of visibly uncracked slabs, as seen from Figure 9. The uplift range was 2 ~ 8 mm (0.08 ~ 0.20 in.). Slab rocking and joint slamming were pronounced when truck axles crossed the joints. An example of best curve fitting for slab uplift through finite element analysis [ISLAB (*26*)] is shown in Figure 9, with backcalculated total equivalent temperature gradient (*27*) values ΔT_{total} listed. The modeling parameters in ISLAB are as follows: slab is 254 mm (10 in.) in thickness and 4.57 m (15 ft) in length; Young's modulus is 27.6 MPa (4×10^{-6} psi); coefficient of thermal expansion of concrete is 10×10^{-6}/°C (5.6×10^{-6}/°F); and the modulus of subgrade reaction k is 68 kPa/mm (250 pci).

As shown in Figure 9, ΔT_{total} ranges from –28°C to –42°C, accounting for the combined effect of built-in curl, daily temperature curl and moisture warping. For Michigan environmental conditions, daily temperature gradient typically ranges from –6 °C ~ 8 °C; built-in curl is –11 °C ~ 2 °C (*25*). Thus, the majority of ΔT_{total} is probably from moisture warping in which water absorption at the bottom may dominate. This was further verified by cone penetrometer testing and visual inspection of outlet drains, in which water along the pavement edge was not draining as expected, suggesting that the slab bottom was in contact with water.

CONCLUSIONS

External drying, self-desiccation, and water absorption are the major transport processes affecting concrete pavement moisture history, hence its warping deformations. Results and analysis presented in this paper suggest that the total moisture loss is a result of both self-desiccation and external drying. Self-desiccation and pore-discontinuity render slabs on grade prone to excessive moisture warping uplift at the joints if the slab bottom is in contact with water for extended periods.

A methodology is proposed for calculating moisture-related deformations based on a relationship established from autogenous shrinkage results. In this relationship, concrete shrinkage deformation is found to be a function of internal pore humidity of cement paste and volumetric aggregate concentration. An equivalent temperature gradient ΔT_e is proposed to characterize moisture effect and to facilitate postprocessing of moisture-related deformation and stresses. The proposed method enables estimating joint movement and warping deformation if moisture state and concrete mix of a slab on grade are known.

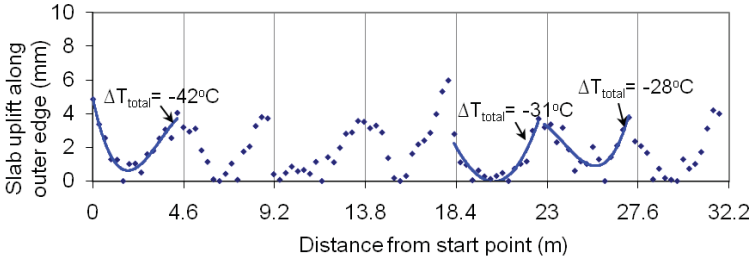

FIGURE 9 Surface elevation profiles for WB I-96 JPCP, CS 47065, with corresponding total equivalent temperature gradient values listed (*21*).

ACKNOWLEDGMENT

This material is based on work supported by the National Science Foundation and the Michigan Department of Transportation as part of the Pavement Research Center of Excellence project, PCC Pavement Acceptance Criteria for New Construction When Built-In Curling Exists.

REFERENCES

1. Poblete, M., A. Garcia, J. David, P. Ceza, and R. Espinosa. Moisture Effects on the Behavior of PCC Pavements. *Proc., 2nd International Workshop on the Design and the Evaluation of Concrete Pavements*, Siguenza, Spain, 1990.
2. Darter, M. I., K. T. Hall, and C.-M. Kuo. *NCHRP Report 372: Support Under Portland Cement Concrete Pavements.* TRB, National Research Council, Washington, D.C., 1995.
3. Ytterberg, R. F. Shrinkage and Curling of Slabs on Grade: Part III—Additional Suggestions. *Concrete International*, Vol. 9, June 1987, pp. 72–81.
4. Suprenant, B. A. Why Slabs Curl: Part II—Factors Affecting the Amount of Curling. *Concrete International*, Vol. 24, No. 4, 2002, pp. 59–74.
5. Powers, T. C., and T. L. Brownyard. Studies of the Physical Properties of Hardened Portland Cement Paste. *Proc., ACI*, Vol. 43, 1947, pp. 971–992.
6. Powers, T. C., L. E. Copeland, and H. M. Mann. Capillary Continuity or Discontinuity in Cement Paste. *PCA Bulletin*, Vol. 10, 1959, pp. 2–12.
7. Hall, C. Water Sorptivity of Mortars and Concretes: A Review. *Magazine of Concrete Research*, Vol. 41, No. 147, 1989, pp. 51–61.
8. Martys, N. S., and C. F. Ferraris. Capillary Transport in Mortars and Concrete. *Cement and Concrete Research*, Vol. 27, No. 5, 1997, pp. 747–760.
9. Koenders, E. A. B. *Simulation of Volume Changes in Hardening Cement-Based Materials.* PhD thesis. Delft University of Technology, Delft, Netherlands, 1997.
10. Nilsson, L. O., and K. A. Mjornell. A Macro-Model for Self-Desiccation in High Performance Concrete. Report TVBM-3126. *Proc., 4th International Research Seminar on Self-Desiccation and Its Importance in Concrete Technology*, Gaithersburg, Md., 2005, pp. 49–66.
11. Jensen, O. M. Thermodynamic Limitation of Self-Desiccation. *Cement and Concrete Research*, Vol. 25, No. 1, 1995, pp. 157–164.
12. Mindess, S., J. F. Young, and D. Darwin. *Concrete*, 2nd ed. Pearson Education, Inc., Upper Saddle River, N.J., 2003.
13. Janssen, D. J. Moisture in Portland Cement Concrete. In *Transportation Research Record 1121*, TRB, National Research Council, Washington, D.C., 1987, pp. 40–44.
14. Neithalath, N. Analysis of Moisture Transport in Mortars and Concrete Using Sorption-Diffusion Approach. *ACI Materials Journal*, Vol. 103, No. 3, 2006, pp. 209–217.
15. Hveem, F. N. Slab Warping Affects Pavement Joint Performance. *Journal of the American Concrete Institute*, June 1951, pp. 797–809.
16. Beddoe, R., and R. Springenschmid. Moisture Transport Through Concrete Structural Components. *Beton- und Stahlbetonbau*, Vol. 94, No. 4, 1999, pp. 158–166.
17. *CEB-FIP Model Code 1990: Design Code*. Thomas Telford, London, 1993.
18. Bazant, Z. P., and S. Baweja. *Creep and Shrinkage Prediction Model for Analysis and Design of Concrete Structures: Model B3*, ACI SP-194. American Concrete Institute, Farmington Hills, Mich., 2001, pp. 1–83.
19. Jonasson, J.-E., P. Groth, and H. Hedlund. Modeling of Temperature and Moisture Field in Concrete to Study Early Age Movements as a Basis for Stress Analysis. *Thermal Cracking in Concrete at Early Ages: Proceedings of the International RILEM Symposium*, Spon Press, London, 1994, pp. 45–54.
20. Wei, Y., W. Hansen, J. J. Biernacki, and E. Schlangen Unified Shrinkage Model for Concrete from Autogenous Shrinkage Test on Paste With and Without GGBFS. *ACI Materials Journal*, Vol. 108, No. 1, 2010, pp. 13–20.
21. Kosmatka, S. H., H. Kerkhoff, and W. C. Panarese. *Design and Control of Concrete Mixtures*, 14th ed. EB001. Portland Cement Association, Skokie, Ill., 2002.
22. Pickett, G. Effect of Aggregate on Shrinkage of Concrete and Hypothesis Concerning Shrinkage. *Journal of the American Concrete Institute*, Vol. 56, No. 1, 1956, pp. 581–590.
23. L'Hermite, R. G. Volume Changes of Concrete. *Proc., 4th International Symposium on the Chemistry of Cement*, Washington, D.C., National Bureau of Standards, U.S. Department of Commerce, 1960, pp. 659–702.
24. Springenschmid, R., and M. Plannerer. *Experimental Research on the Test Methods for Surface Cracking of Concrete.* Institute for Building Materials, Technical University Munich, Germany, 2001.
25. Hansen, W., and Y. Wei. *PCC Pavement Acceptance Criteria for New Construction When Built-In Curling Exists.* MDOT Report No. RC-1481. Michigan Department of Transportation, Ann Arbor, 2008.
26. Khazanovich, L., H. T. Yu, S. Rao, K. Galasova, E. Shats, and R. Jones. *ISLAB2000—Finite Element Analysis Program for Rigid and Composite Pavements. User's Guide.* ERES Division of Applied Research Associates, Inc., Champaign, Ill., 2000.
27. Ruiz, J. M., P. J. Kim, A. K. Schindler, and R. O. Rasmussen. Validation of HIPERPAV for Prediction of Early-Age Jointed Concrete Pavement Behavior. In *Transportation Research Record: Journal of the Transportation Research Board, No. 1778*, TRB, National Research Council, Washington, D.C., 2001, pp. 17–25.

This paper does not constitute a standard, specification, or regulation. Any opinions, findings, and conclusions or recommendations expressed in this material are those of the authors and do not necessarily reflect the views of the National Science Foundation or the Michigan Department of Transportation.

The Basic Research and Emerging Technologies Related to Concrete Committee peer-reviewed this paper.